Supplementary Material

Doping and Heterojunction Strategies for Constructing V-doped Ni_3FeN/Ni Anchored on N-doped Graphene Tubes as Efficient Overall Water Splitting Electrocatalyst

Guanying Song[a], Siqi Luo[a], Qing Zhou[a], Jiachen Zou[a], ,Yusheng Lin[a], Lei Wang[b], Guicun Li[a], Alan Meng[*b] Zhenjiang Li[*a]

[a]*College of Electromechanical Engineering, College of Materials Science and Engineering, Qingdao University of Science and Technology, Qingdao 266061, P. R. China.*

[b] *Key Laboratory of Optic-electric Sensing and Analytical Chemistry for Life Science, MOE, College of Chemistry and Molecular Engineering, Qingdao University of Science and Technology, Qingdao 266042, Shandong, P. R. China.*

* Corresponding author. Tel.: +86 532 88959506; fax: +86 532 88959506.

E-mail address: alanmengqust@163.com (A. L. Meng);

zhenjiangli@qust.edu.cn (Z. J. Li)

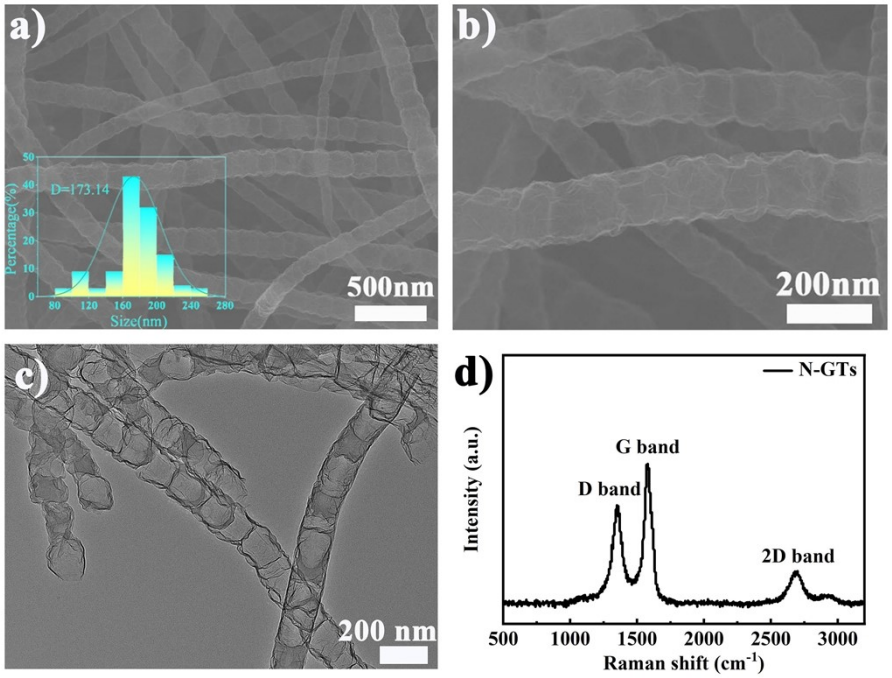

Fig. S1. (a, b) SEM image, (the inset in (a) is the diameter distribution of the N-GTs), (c) TEM image, (d) Raman spectra of self-synthesized N-GTs.

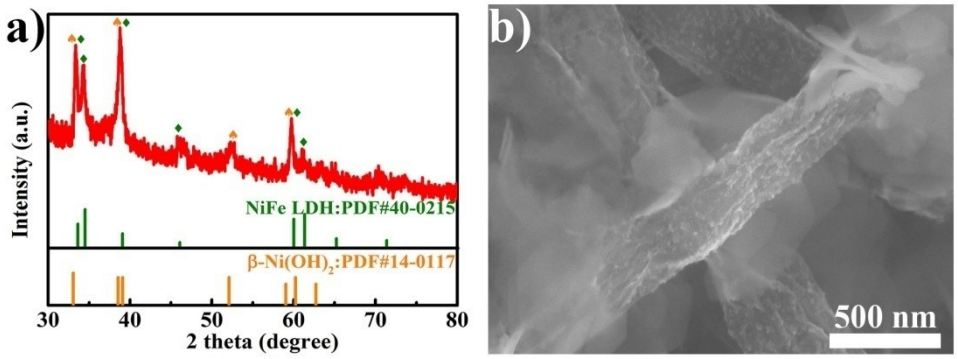

Fig. S2. (a) XRD pattern, (b) SEM image of V-doping Ni-Fe precursor prepared by hydrothermal method.

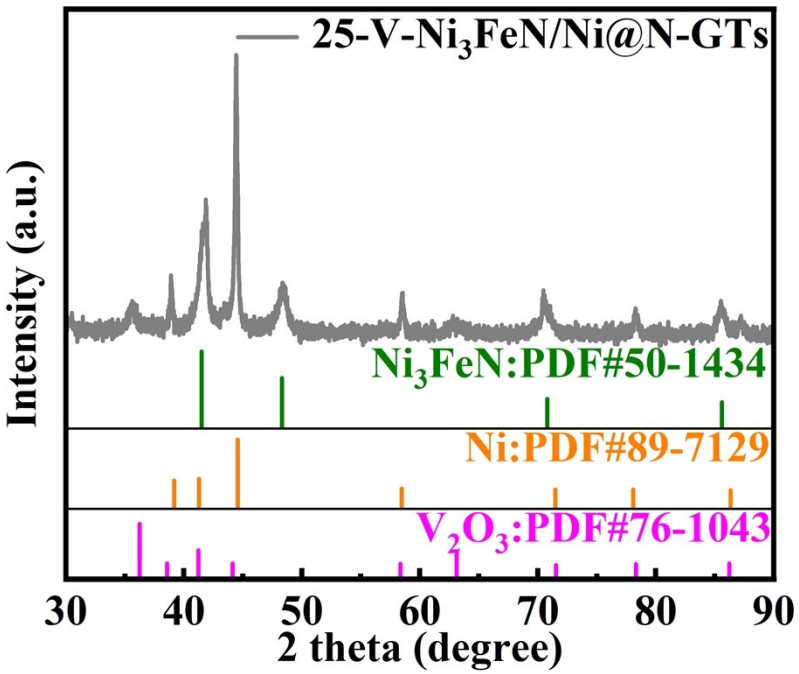

Fig. S3. XRD of 25-V-Ni_3FeN/Ni@N-GTs.

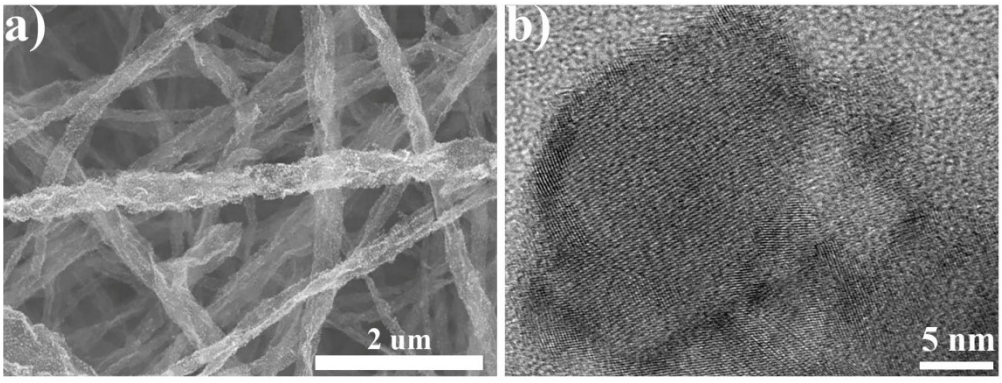

Fig. S4. (a) SEM image, (b) HRTEM image of V-Ni_3FeN/Ni@N-GTs.

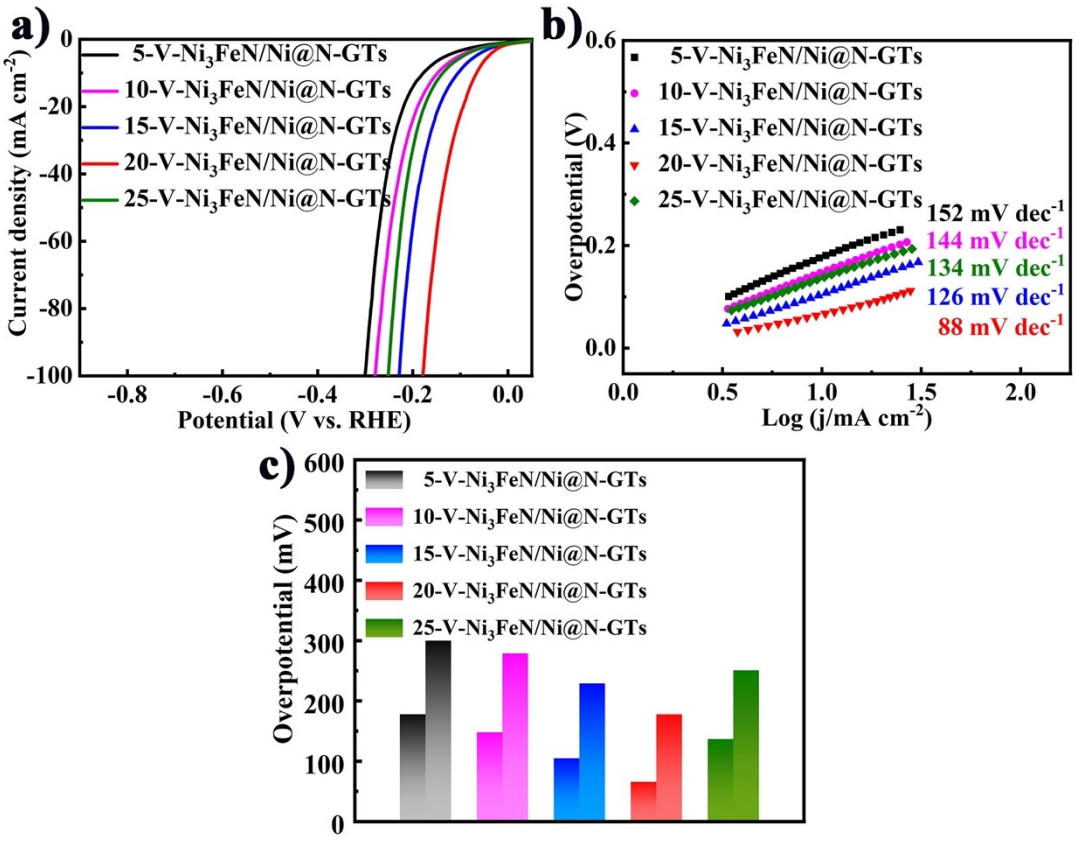

Fig. S5. Electrocatalysis of the HER in alkaline media: a) LSV curves b) Corresponding overpotentials at the current density of 10 mA cm^{-2} and 100 mA cm^{-2} c) Tafel plots of 5-V-Ni$_3$FeN/Ni@N-GTs, 10-V-Ni$_3$FeN/Ni@N-GTs, 15-V-Ni$_3$FeN/Ni@N-GTs, 20-V-Ni$_3$FeN/Ni@N-GTs and 25-V-Ni$_3$FeN/Ni@N-GTs.

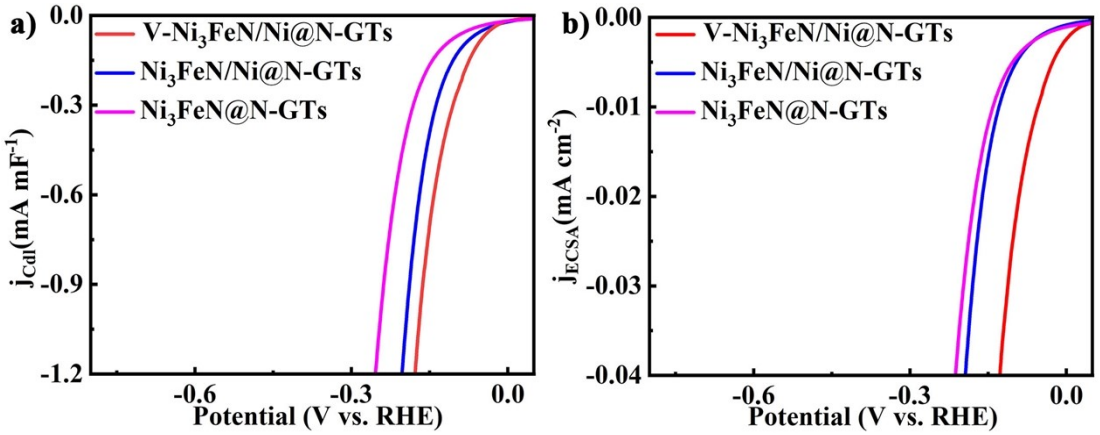

Fig. S6. LSV curves of HER normalized by (a) the electrochemical double-layer capacitance C_{dl} and (b) the electrochemical active surface area (ECSA).

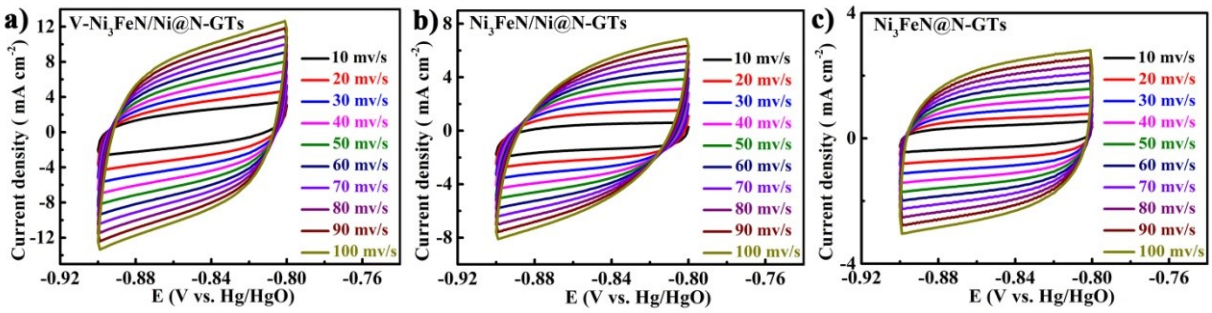

Fig. S7. CVs performed at various scan rates in the region of -0.90 V to -0.8 V (vs. Hg/HgO) for (a) V-Ni_3FeN/Ni @N-GTs, (b) Ni_3FeN/Ni@N-GTs, (c)Ni_3FeN@N-GTs.

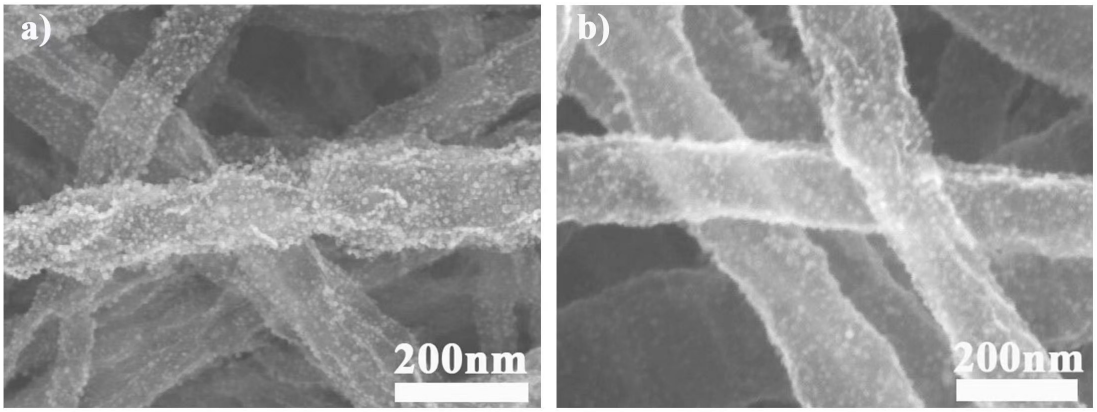

Fig. S8. SEM images of the V-Ni_3FeN/Ni@N-GTs before (a) and after (b) HER stability testing.

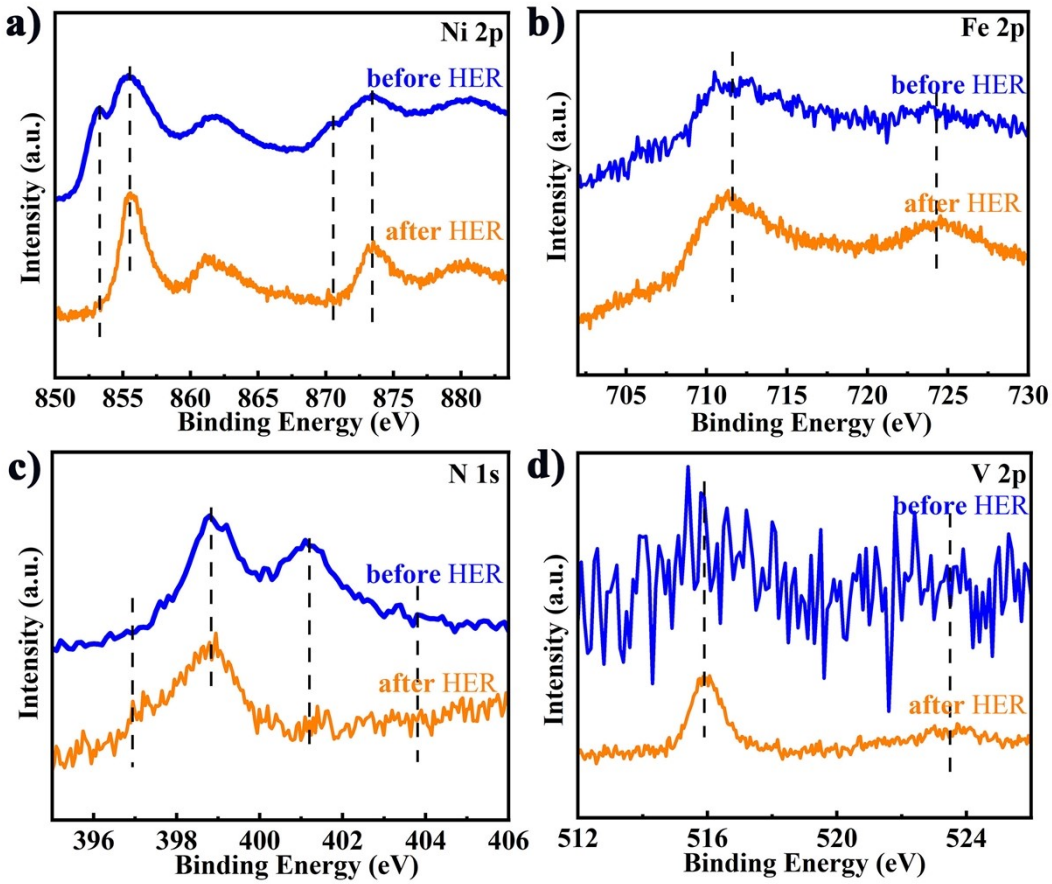

Fig. S9. The XPS spectra of V-Ni_3FeN/Ni@N-GTs before and after HER test.

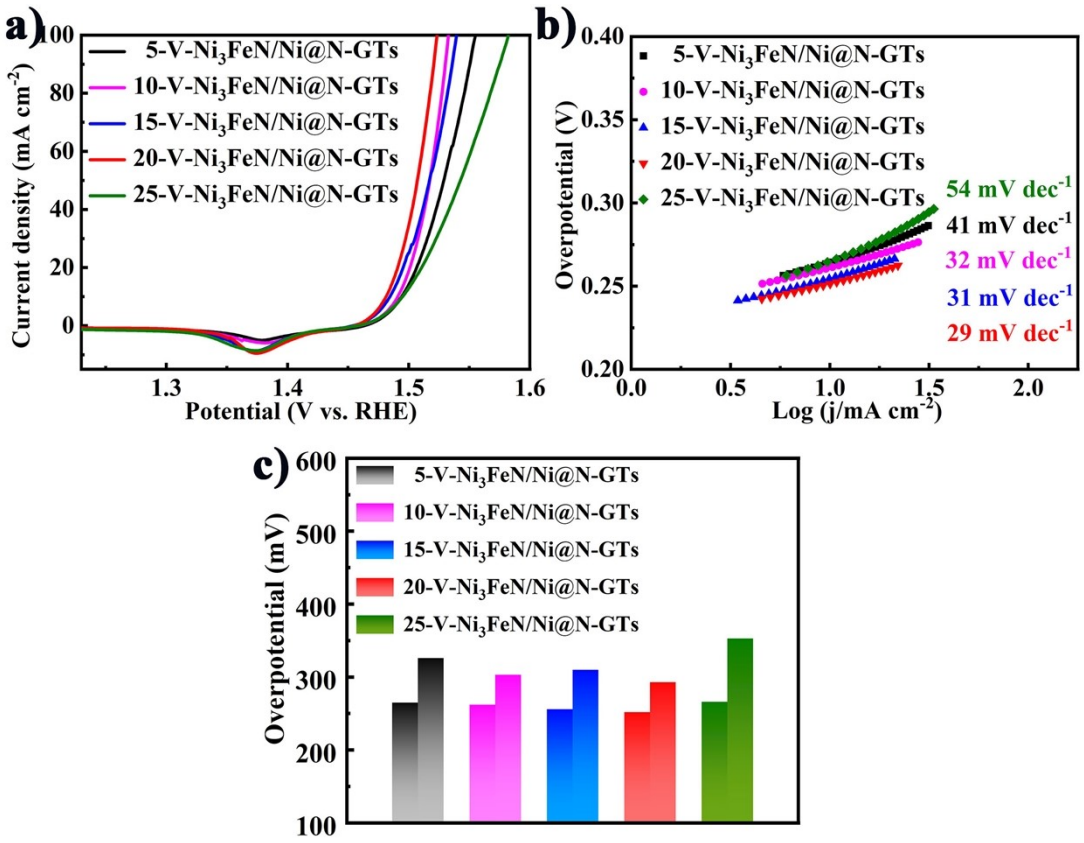

Fig. S10. Electrocatalysis of the OER in alkaline media: a) LSV curves b) Corresponding overpotentials at the current density of 10 mA cm^{-2} and 100 mA cm^{-2} c) Tafel plots of 5-V-Ni$_3$FeN/Ni@N-GTs, 10-V-Ni$_3$FeN/Ni@N-GTs, 15-V-Ni$_3$FeN/Ni@N-GTs, 20-V-Ni$_3$FeN/Ni@N-GTs and 25-V-Ni$_3$FeN/Ni@N-GTs.

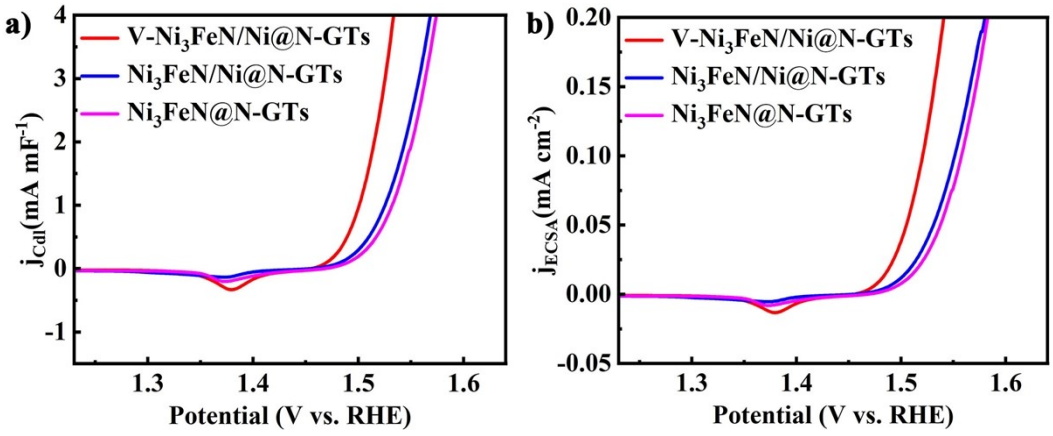

Fig. S11. LSV curves of OER normalized by a) the electrochemical double-layer capacitance Cdl and b) the electrochemical active surface area ECSA.

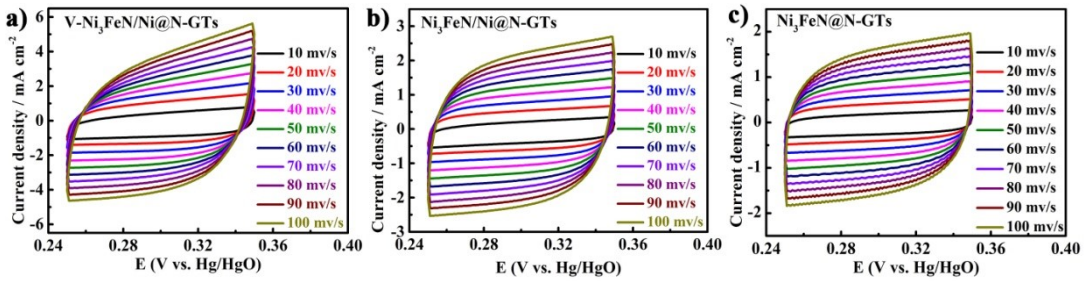

Fig. S12. CVs performed at various scan rates in the region of 0.25 V to 0.35 V (vs. Hg/HgO) for (a) V-Ni_3FeN/Ni@N-GTs, (b) Ni_3FeN/Ni@N-GTs, (c)Ni_3FeN@N-GTs.

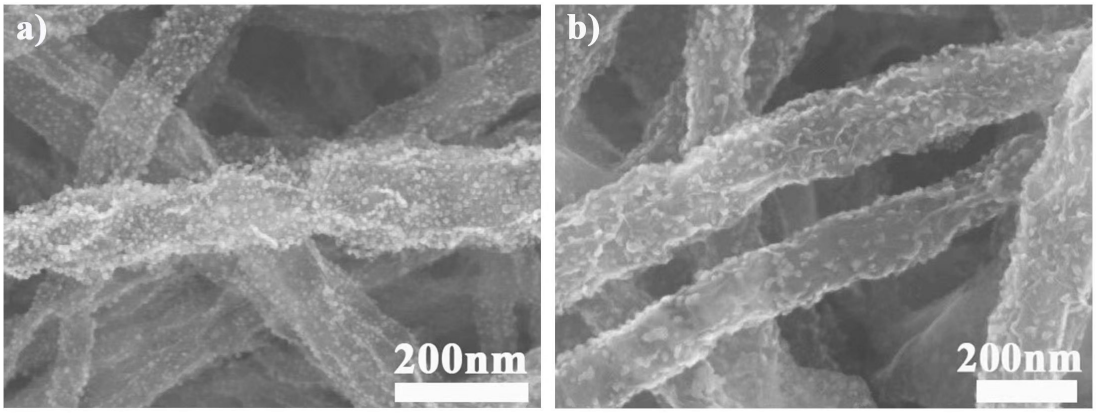

Fig. S13. SEM images of the V-Ni_3FeN/Ni@N-GTs before (a) and after (b) OER stability testing.

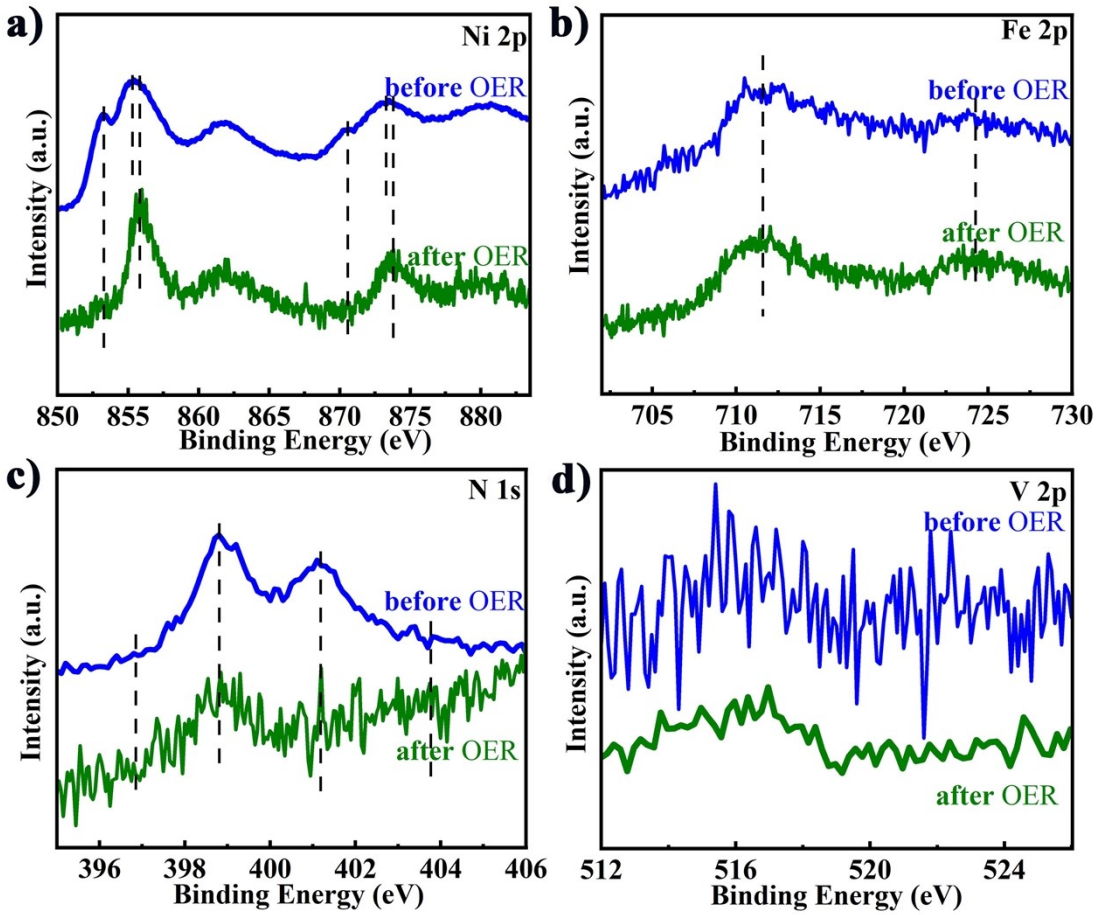

Fig. S14. The XPS spectra of V-Ni_3FeN/Ni@N-GTs before and after OER test.

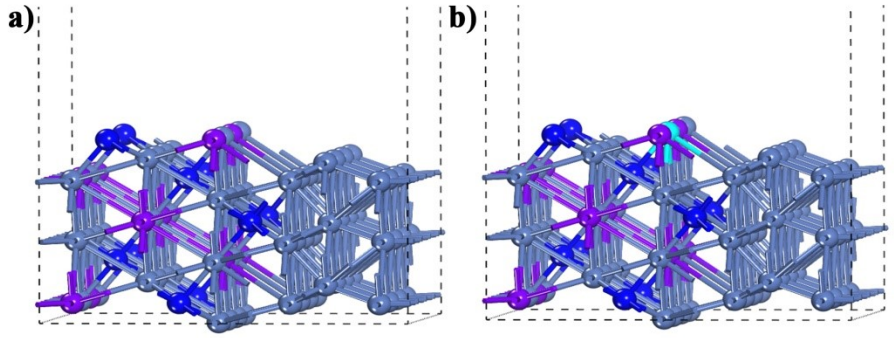

Fig. S15. The optimized model structure diagram of (a) Ni_3FeN/Ni and (b) V-Ni_3FeN/Ni.

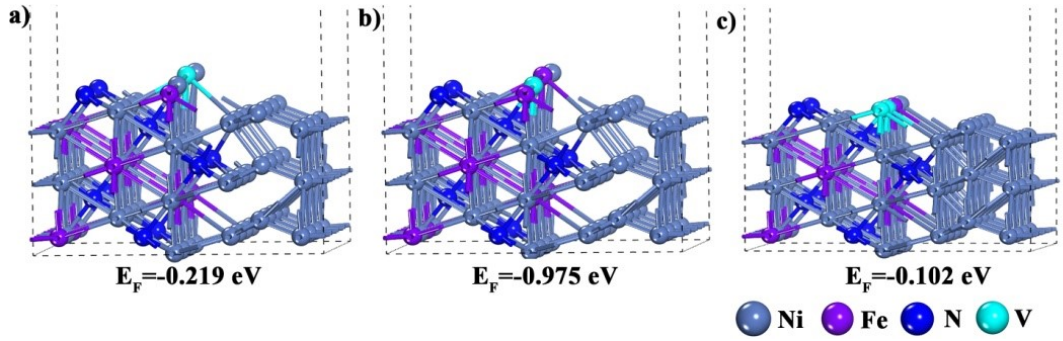

Fig. S16. Structures and formation energies (E_{tot}) of (a) V substitute Fe, (b) V substitute Ni, (c) V substitute Fe and Ni in the V-Ni_3FeN/Ni material.

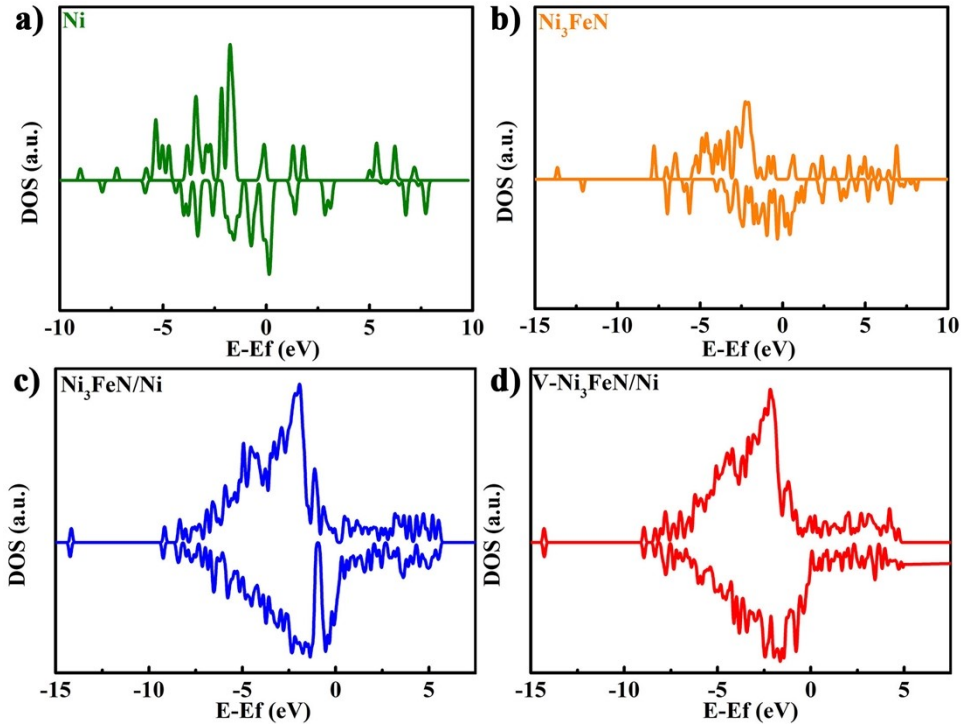

Fig. S17. Density of states on (a) Ni, (b) Ni_3FeN, (c) Ni_3FeN/Ni and (d) V-Ni_3FeN/Ni.

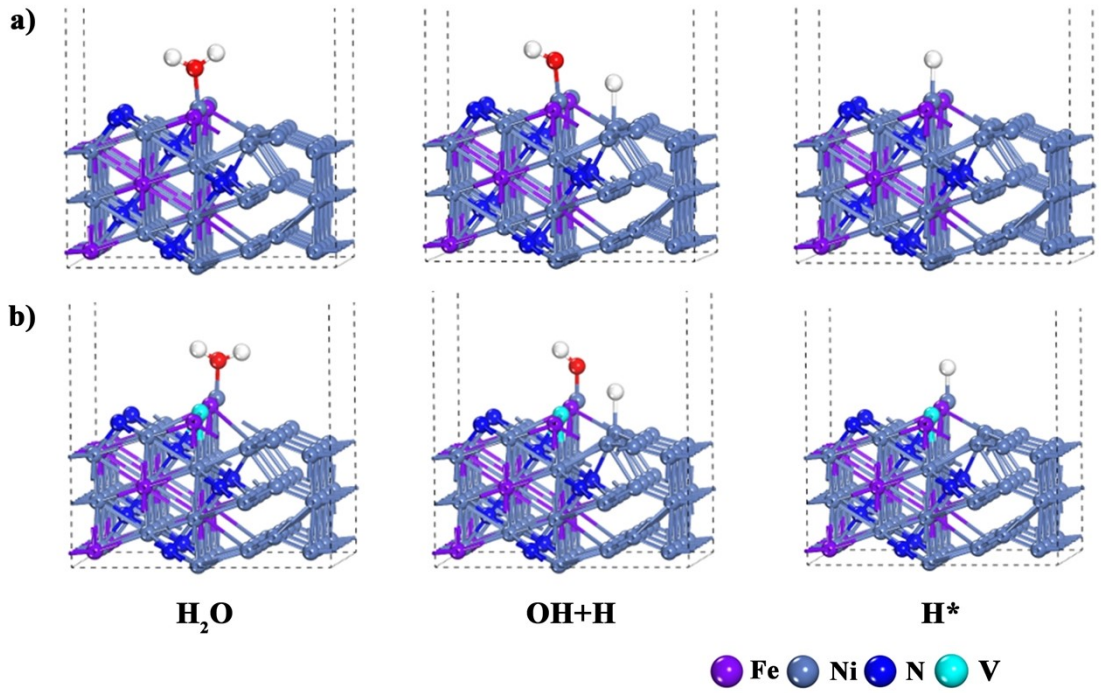

Fig. S18. Side view of schematic structural representations for water dissociation and hydrogen adsorption at Ni site in the pristine Ni_3FeN/Ni (a) and V-Ni_3FeN/Ni (b).

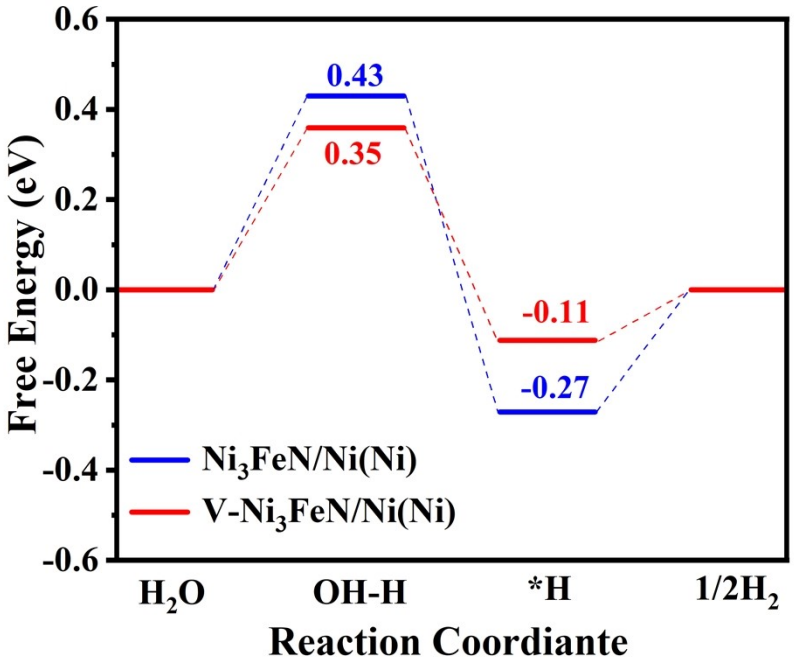

Fig. S19. Free energy diagrams for alkaline HER on V-Ni_3FeN/Ni@N-GTs and Ni_3FeN/Ni@N-GTs.

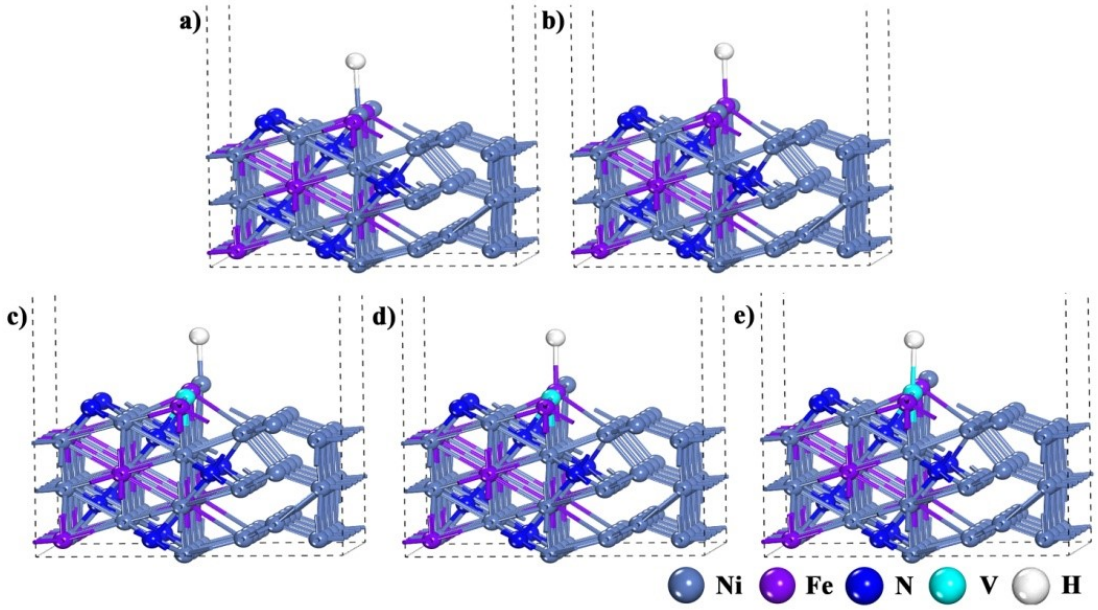

Fig. S20 Side view of schematic structural representations for hydrogen adsorption at Ni and Fe sites in the pristine Ni_3FeN/Ni (a-b); Side view of schematic structural representations for hydrogen adsorption at Ni, Fe and V sites in V-Ni_3FeN/Ni (c-e).

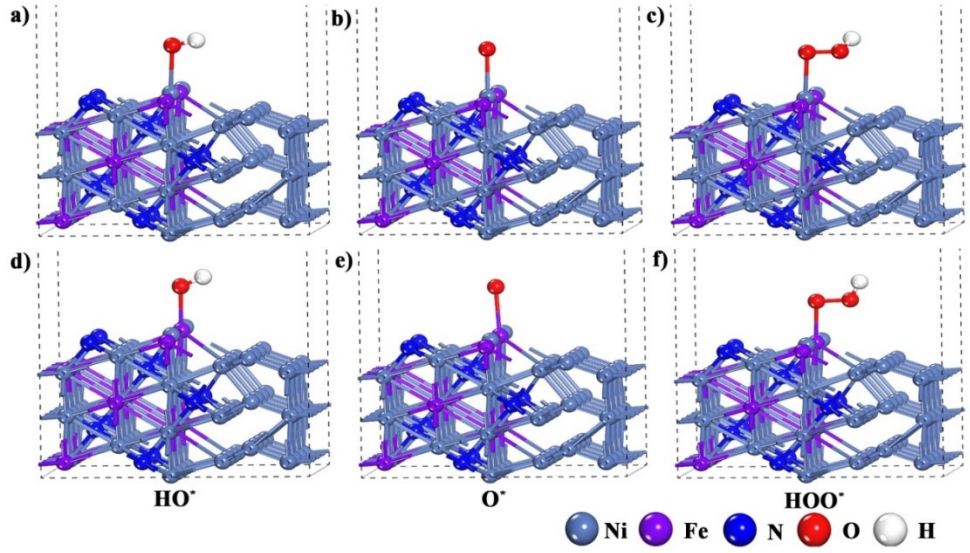

Fig. S21. Side view of schematic structural representations for oxygen adsorption at Ni and Fe sites in the pristine Ni_3FeN/Ni.

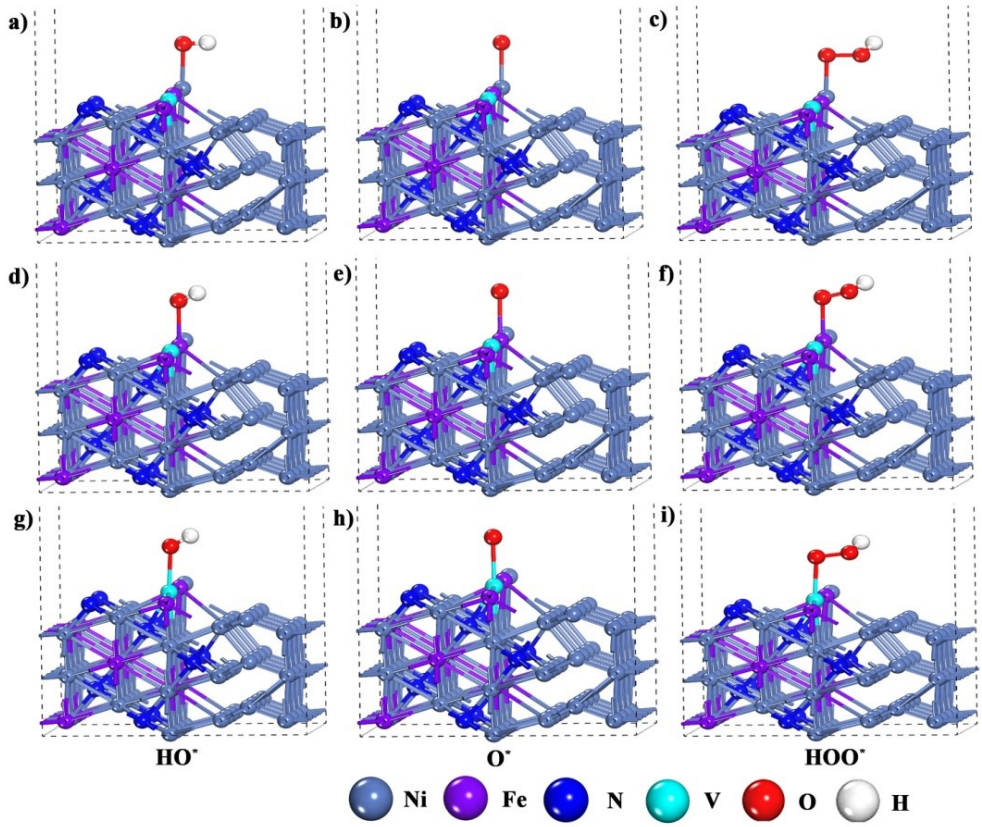

Fig. S22. Side view of schematic structural representations for oxygen adsorption at Ni, Fe and V sites in V-Ni_3FeN/Ni.

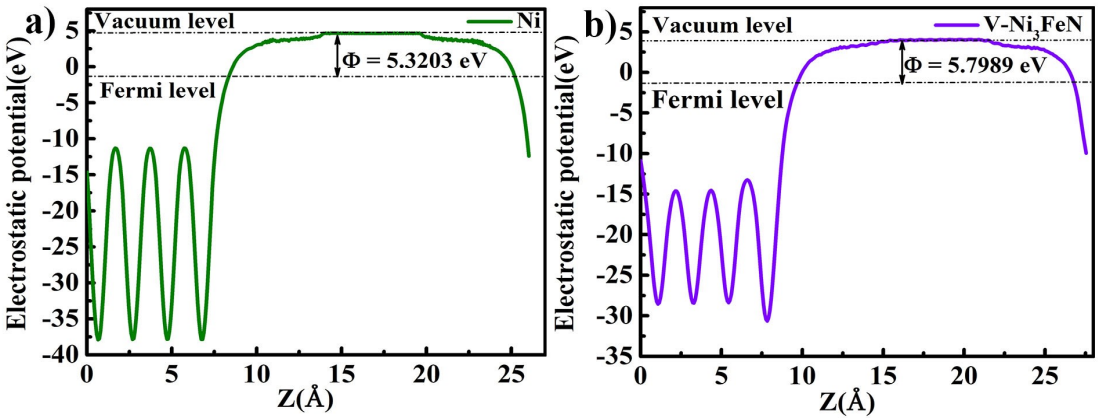

Fig. S23. The work function values of (a) Ni and (b) V-Ni_3FeN.

Tab. S1. HER performance of different catalysts in alkaline solution (1M KOH).

Catalyst	Overpotential / mV ($10\ mA\ cm^{-2}$)	Tafel slop ($mV\ dec^{-1}$)	Electrolyte	Ref
V-Ni_3FeN/Ni@N-GTs	66	88	1.0 M KOH	This work
NiCo	86	62.1	1.0 M KOH	[1]
Ni_3S_2@NGCLs/NF	134	84	1.0 M KOH	[2]
Ni_2P–$Ni_{12}P_5$	76	68	1.0 M KOH	[3]
d-Ni_3FeN/Ni_3Fe	125	98	1.0 M KOH	[4]
$CoNi_2S_4$/WS_2/Co_9S_8	70	112	1.0 M KOH	[5]
Fe-Ni_5P_4/NiFeOH	197	94	1.0 M KOH	[6]
Mo-$NiCo_2O_4$/$Co_{5.47}N$/NF	81	116.7	1.0 M KOH	[7]
CoO_x/CoN_y@CN_z	261	84	1.0 M KOH	[8]
Ni_2P/Ni_3S_2	79	50.4	1.0 M KOH	[9]
Ni@NC6-600	181	119	1.0 M KOH	[10]

Tab. S2.OER performance of different catalysts in alkaline solution (1M KOH).

Catalyst	Overpotential / mV (10 mA cm^{-2})	Tafel slop (mV dec^{-1})	Electrolyte	Ref
V-Ni_3FeN/Ni@N-GTs	252	29	1.0 M KOH	This work
Ni_3S_2@NGCLs/NF	271	99	1.0 M KOH	[2]
$NiCo_2O_4$@CoS/NF	290	92	0.1 M KOH	[11]
NiCoFe-MOF-74	273	63	0.1 M KOH	[12]
NiCoPO/NC	300	94	1.0 M KOH	[13]
CoNS/C	345	83.3	1.0 M KOH	[14]
NiMoNS	260	54.7	1.0 M KOH	[15]
Ni/$NiFe_2O_4$-CNTs	284	46.3	1.0 M KOH	[16]
Fe@BIF-73-NS	291	37.9	1.0 M KOH	[17]
V-$NiCo_2O_4$	340	71.9	1.0 M KOH	[18]
$(Co_{1-x}Fe_x)_9S_8$	268	63.9	1.0 M KOH	[19]

Tab. S3. Overall water split ing performance of different catalysts in alkaline solution (1 M KOH).

Catalyst	Overpotential / mV (10 mA cm^{-2})	Electrolyte	Ref
V-Ni_3FeN/Ni@N-GTs||V-Ni_3FeN/Ni@N-GTs	1.55	1.0 M KOH	This work
CdS@Co_9S_8/Ni_3S_2||CdS@Co_9S_8/Ni_3S_2	1.56	1.0 M KOH	[20]
NiFe-LDH/$Ni(OH)_2$||NiFe-LDH/$Ni(OH)_2$	1.60	1.0 M KOH	[21]
Mo-$NiCo_2O_4$/$Co_{5.47}N$/NF||Mo-$NiCo_2O_4$/$Co_{5.47}N$/NF	1.56	1.0 M KOH	[7]
CoO_x/CoN_y@CN_z||CoO_x/CoN_y@CN_z	1.57	1.0 M KOH	[8]
$NiCo_2O_4$@NiS || $NiCo_2O_4$@NiS	1.65	1.0 M KOH	[22]
d-Ni_3FeN/Ni_3Fe||d-Ni_3FeN/Ni_3Fe	1.61	1.0 M KOH	[4]
Ni_3S_2/Cu-NiCo LDH/NF|| Ni_3S_2/Cu-NiCo LDH/NF	1.58	1.0 M KOH	[23]
$FeCoP_2$@NPPC||$FeCoP_2$@NPPC	1.6	1.0 M KOH	[24]
P-Fe_3N@NC NSs/IF||P-Fe_3N@NC NSs/IF	1.61	1.0 M KOH	[25]
NiFeOP||NiFeOP	1.57	1.0 M KOH	[26]

References

[1] J. Zhou, L. Yu, Q. Zhou, C. Huang, Y. Zhang, B. Yu, Y. Yu, Ultrafast fabrication of porous transition metal foams for efficient electrocatalytic water splitting, Appl. Catal. B: Environ. 288 (2021) 120002.

[2] B. Li, Z. Li, Q. Pang, J. Zhang, Core/shell cable-like Ni_3S_2 nanowires/N-doped graphene-like carbon layers as composite electrocatalyst for overall electrocatalytic water splitting, Chem. Eng. J. 401 (2020) 126045.

[3] Z. Wang, S. Wang, L. Ma, Y. Guo, J. Sun, N. Zhang, R. Jiang, Water-Induced Formation of Ni_2P–$Ni_{12}P_5$ Interfaces with Superior Electrocatalytic Activity toward Hydrogen Evolution Reaction, Small. 17 (2021) 2006770.

[4] Z. Li, H. Jang, D. Qin, X. Jiang, X. Ji, M.G. Kim, L. Zhang, X. Liu, J. Cho, Alloy-strain-output induced lattice dislocation in Ni_3FeN/Ni_3Fe ultrathin nanosheets for highly efficient overall water splitting, J. Mater. Chem. A. 9 (2021) 4036-4043.

[5] M. Ma, J. Xu, H. Wang, X. Zhang, S. Hu, W. Zhou, H. Liu, Multi-interfacial engineering of hierarchical $CoNi_2S_4$/WS_2/Co_9S_8 hybrid frameworks for robust all-pH electrocatalytic hydrogen evolution, Appl. Catal. B: Environ. 297 (2021) 120455.

[6] C. Li, J. Zhao, L. Xie, J. Wu, G. Li, Fe doping and oxygen vacancy modulated Fe-Ni_5P_4/NiFeOH nanosheets as bifunctional electrocatalysts for efficient overall water splitting, Appl. Catal. B: Environ. 291 (2021) 119987.

[7] W. Liu, L. Yu, R. Yin, X. Xu, J. Feng, X. Jiang, D. Zheng, X. Gao, X. Gao, W. Que, P. Ruan, F. Wu, W. Shi, X. Cao, Non-3d Metal Modulation of a 2D Ni–Co Heterostructure Array as Multifunctional Electrocatalyst for Portable Overall Water Splitting, Small. 16 (2020) 1906775.

[8] J. Liu, C. Wang, H. Sun, H. Wang, F. Rong, L. He, Y. Lou, S. Zhang, Z. Zhang, M. Du, CoO_x/CoN_y nanoparticles encapsulated carbon-nitride nanosheets as an efficiently trifunctional electrocatalyst for overall water splitting and Zn-air battery, Appl. Catal. B: Environ. 279 (2020) 119407.

[9] H. Su, S. Song, S. Li, Y. Gao, L. Ge, W. Song, T. Ma, J. Liu, High-valent bimetal Ni_3S_2/Co_3S_4 induced by Cu doping for bifunctional electrocatalytic water splitting, Appl. Catal. B: Environ. 293 (2021) 120225.

[10] N. Cheng, N. Wang, L. Ren, G. Casillas-Garcia, N. Liu, Y. Liu, X. Xu, W. Hao, S.X. Dou, Y. Du, In-situ grafting of N-doped carbon nanotubes with Ni encapsulation onto MOF-derived hierarchical hybrids for efficient electrocatalytic hydrogen evolution, Carbon. 163 (2020) 178-185.

[11] S. Adhikari, Y. Kwon, D.-H. Kim, Three-dimensional core–shell structured $NiCo_2O_4$@CoS/Ni-Foam electrocatalyst for oxygen evolution reaction and electrocatalytic oxidation of urea, Chem. Eng. J. 402 (2020) 126192.

[12] H. Zheng, Y. Wang, P. Zhang, F. Ma, P. Gao, W. Guo, H. Qin, X. Liu, H. Xiao, Multiple effects driven by AC magnetic field for enhanced electrocatalytic oxygen evolution in alkaline electrolyte, Chem. Eng. J. 426 (2021) 130785.

[13] C. Wang, W. Chen, D. Yuan, S. Qian, D. Cai, J. Jiang, S. Zhang, Tailoring the nanostructure and electronic configuration of metal phosphides for efficient electrocatalytic oxygen evolution reactions, Nano Energy. 69 (2020) 104453.

[14] Y. Wang, S. Zhang, X. Meng, T. Wang, Y. Feng, W. Zhang, Y. He, Y. Huang, N. Yang, Z.-F. Ma, Surface Tuning to Promote the Electrocatalysis for Oxygen Evolution Reaction: From Metal-Free to Cobalt-Based Carbon Electrocatalysts, ACS Appl. Mater. Interfaces. 13 (2021) 503-513.

[15] Y. Liu, P. Liu, Y. Men, Y. Li, C. Peng, S. Xi, Y. Pan, Incorporating MoO_3 Patches into a Ni Oxyhydroxide Nanosheet Boosts the Electrocatalytic Oxygen Evolution Reaction, ACS Appl. Mater. Interfaces. 13 (2021) 26064-26073.

[16] X. Yu, G. Chen, Y. Wang, J. Liu, K. Pei, Y. Zhao, W. You, L. Wang, J. Zhang, L. Xing, Hierarchical coupling effect in hollow Ni/$NiFe_2O_4$-CNTs microsphere via spray-drying for enhanced oxygen evolution electrocatalysis, Nano Res. 13 (2020) 437-446.

[17] T. Wen, M. Liu, S. Chen, Q. Li, Y. Du, T. Zhou, C. Ritchie, J. Zhang, 2D Boron Imidazolate Framework Nanosheets with Electrocatalytic Applications for Oxygen Evolution and Carbon Dioxide Reduction Reaction, Small. 16 (2020) 1907669.

[18] X. Wang, Y. Zhou, J. Luo, F. Sun, J. Zhang, Synthesis of V-doped urchin-like $NiCo_2O_4$ with rich oxygen vacancies for electrocatalytic oxygen evolution reactions, Electrochim. Acta. 406 (2022) 139800.

[19] Y. Wang, Z. Meng, X. Gong, C. Jiang, C. Zhang, J. Xu, Y. Li, J. Bao, Y. Cui, H. Wang, Y. Zeng, X. Hu, S. Yu, H. Tian, Enhancing stability of Co_9S_8 by iron incorporation for oxygen evolution reaction and supercapacitor electrodes, Chem. Eng. J. 431 (2022) 133980.

[20] F. Si, C. Tang, Q. Gao, F. Peng, S. Zhang, Y. Fang, S.J.J.o.M.C.A. Yang, Bifunctional CdS@ Co_9S_8/Ni_3S_2 catalyst for efficient electrocatalytic and photo-assisted electrocatalytic overall water splitting, J. Mater. Chem. A. 8 (2020) 3083-3096.

[21] N. Gultom, H. Abdullah, C. Hsu, D. Kuo, Activating nickel iron layer double hydroxide for alkaline hydrogen evolution reaction and overall water splitting by electrodepositing nickel hydroxide, Chem. Eng. J. 419 (2021) 129608.

[22] L. Feng, W. Lu, J. Liu, D. Li, L. Hu, C. Xu, Guarding active sites and electron transfer engineering of core-shell nanosheet as robust bifunctional applications for overall water splitting and capacitors, Electrochim. Acta. 331 (2020) 135372.

[23] L. Jia, G. Du, D. Han, Y. Hao, W. Zhao, Y. Fan, Q. Su, S. Ding, B. Xu, Ni_3S_2/Cu–NiCo LDH heterostructure nanosheet arrays on Ni foam for electrocatalytic overall water splitting, J. Mater. Chem. A. 9 (2021) 27639-27650.

[24] Y. Wang, Z. Yang, D. Yang, L. Zhao, X. Shi, G. Yang, B. Han, $FeCoP_2$ Nanoparticles Embedded in N and P Co-doped Hierarchically Porous Carbon for Efficient Electrocatalytic Water Splitting, ACS Appl. Mater.

Interfaces. 13 (2021) 8832-8843.

[25] G. Li, J. Yu, W. Yu, L. Yang, X. Zhang, X. Liu, H. Liu, W. Zhou, Phosphorus-Doped Iron Nitride Nanoparticles Encapsulated by Nitrogen-Doped Carbon Nanosheets on Iron Foam In Situ Derived fromSaccharomycetes Cerevisiaefor Electrocatalytic Overall Water Splitting, Small. 16 (2020) 2001980.

[26] Y. Xie, B. Zhao, K. Tang, W. Qin, C. Tan, J. Yao, Y. Li, L. Jiang, X. Wang, Y. Sun, In-situ phase transition induced nanoheterostructure for overall water splitting, Chem. Eng. J. 409 (2021) 128156.